Equivalent Circuit Model of RF Power Detection with AlGaN/GaN HEMTs up to 67 GHz

Gaudencio Paz-Martínez[(1)], Sergio García-Sánchez[(1)], Ignacio Íñiguez-de-la-Torre[(1)]
Philippe Artillan[(2)], Tomás González[(1)], Javier Mateos[(1)]
gaupaz@usal.es, sergio_gs@usal.es, indy@usal.es
philippe.artillan@univ-smb.fr, tomasg@usal.es, javierm@usal.es.
[(1)]Applied Physics Department, and USAL-NANOLAB, Universidad de Salamanca, 37008 Salamanca, Spain.
[(2)] Univ. Grenoble Alpes, Univ. Savoie Mont Blanc, CNRS, Grenoble INP, CROMA, 38000 Grenoble, France.

***Abstract*—The responsivity of zero-bias detectors based on high electron mobility transistors (HEMTs) is studied using measurements up to 67 GHz and a complete small-signal equivalent circuit (SSEC) model, together with a closed-form analytical expression, is used to reproduce the experimental results. The frequency response in drain injection configuration is analyzed as a function of the equivalent circuit elements and the gate bias. The values of the intrinsic and extrinsic elements of the device are compared with those obtained with Monte Carlo simulations of the intrinsic region of the device, showing a very good agreement.**

I. Introduction

Radio frequency (RF) detectors based on GaN high electron mobility transistors (HEMTs) have the ability to operate over a wide temperature [1], [2] and frequency range [3] with a competitive Noise Equivalent Power (NEP) on the order of 10-50 pW/$\sqrt{\text{Hz}}$. They are two-port devices where the signal is injected through one of the ports at a time, but the coupling between gate and drain degrades the response at high frequencies, producing a frequency roll-off of the responsivity [2], [7]. This effect is linked to the small-signal behaviour of the transistors, characterized by their frequency-dependent S-parameter matrix, and therefore can be well reproduced by a small-signal equivalent circuit (SSEC) model of the devices. Assuming that the resistive self-mixing (associated to the device non-linearity) is at the origin of the detection mechanism, such simple model allows predicting the frequency limit for the operation of the devices as its SSEC description can be extended to higher frequencies. At higher frequencies, distributed resistive self-mixing [4], thermoemission processes of plasma-wave effects can also have their contribution [5], but they will not be considered here. In this work we study the response of AlGaN/GaN HEMTs operating as zero bias detectors as a function of gate bias. The frequency roll-off of the detection will be characterized with the -3 dB cut-off frequency (f_{3dB}), for which halved responsivity is obtained. The extraction of the intrinsic and extrinsic elements of the SSEC will be made using the classic Dambrine's method [6] so that a simple circuit simulation can provide the frequency dependent S-parameters which will be inserted into a closed-form analytical expression of the responsivity [7] which allows extrapolating the analysis of the frequency response of the devices at frequencies above the reach of the experimental equipment. Finally the intrinsic elements of the SSEC will also be compared with the results obtained from a Monte Carlo simulation [8] of the device in order to confirm its physical validity. Our tool contains all the ingredients to properly capture the rectification capabilities of such type of transistors.

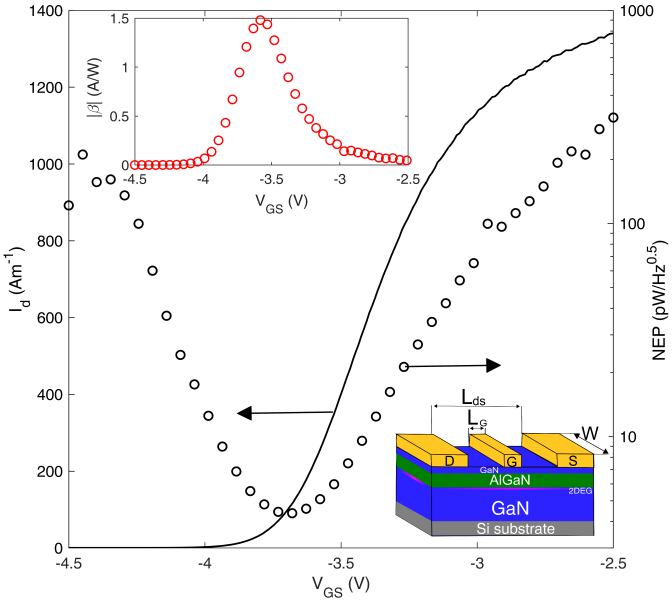

Fig. 1. Transfer I_D-V_{GS} characteristic measured at V_{DS}=0 V of the GaN HEMT (left axis) and the estimated NEP at 1 GHz and T=300 K (right axis). The top inset shows the absolute value of the responsivity at 1 GHz. The bottom inset is an sketch of the transistor geometry.

II. Results and Discussion

A. Device under test and equivalent circuit

The device under test (DUT) is an AlGaN/GaN HEMT grown on a high-resistivity silicon substrate, the layer structure and more details of the fabrication process can be found in [9]–[11]. The bottom inset of the Fig. 1 presents the geometry of the DUT, the gate length and width are L_G=150 nm and W=2×50 μm and the drain-source distance L_{DS}=2.5 μm. The layout contains co-planar-waveguide accesses to contact the terminals with GSG RF probes, the RF source is a Keysight N5247A vector network analyzer up to 67 GHz. In order to bias both the gate and the drain of the transistor, a two-channel

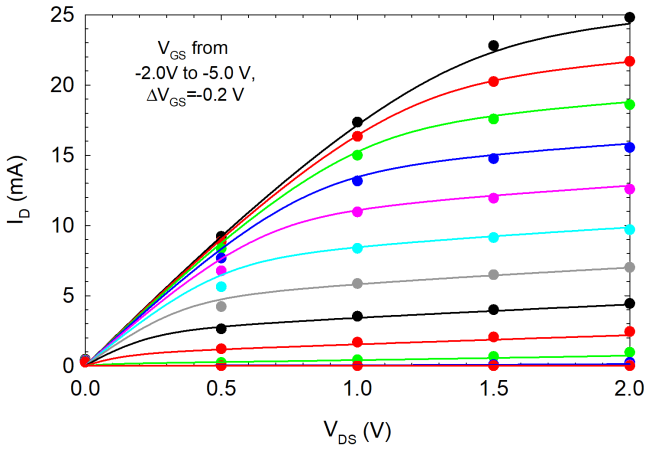

Fig. 2. Comparison of the experimental (lines) output I_D-V_{DS} characteristics with those obtained with MC simulations (circles). The effect of source and drain contact resistances with values R_s=1.6 Ω·mm, R_d=0.3 Ω·mm, respectively (in good agreement with the measured data) and 0.65 eV for the Schottky barrier height at the gate metal-semiconductor junction has been analytically included in the MC simulations.

SMU B2902A is used. The output $I_D - V_{DS}$ characteristics are shown in Fig. 2 and Fig. 1 shows the transfer characteristic I_D-V_{GS} measured at V_{DS}=0.1 V, thus presenting a threshold voltage V_{th}=-3.8 V. The right axis shows the noise equivalent power as a function of gate bias estimated at 1 GHz as NEP=$\frac{\sqrt{4k_BT/R}}{\beta}$ with R the device resistance and β the current responsivity for drain injection (DI) at zero-bias.
In the drain-injection configuration used in our detection experiments, β (in A/W) is obtained as $\beta(f)$=$\Delta I_d(f)/P_{RF}(f)$ being ΔI_d the drain current shift measured when a RF signal of P_{RF} power is injected into the drain port. The absolute value of β is presented in the top inset for P_{RF}=-20 dBm at 1 GHz. As expected, the maximum value of β and the minimum NEP (with excellent values around 1.5 A/W and 5 pW/$\sqrt{\text{Hz}}$, respectively) is obtained for V_{GS} just above V_{th}.

Fig. 3 shown the equivalent circuit of the HEMT [12], with the intrinsic section is closed in the gray box. This SSEC takes into account extrinsic capacitances near the device active region, C_{gd}^{ext}, C_{gs}^{ext} and C_{ds}^{ext}, which are usually included in the intrinsic part of the device model, as well as the classical parasitic elements corresponding to pads and contacts. Since the zero-bias conditions are used in the detection measurements (V_{DS}=0) the value of the transconductance, g_m is taken to be null. Additionally, a R_{gd} resistor is included to the standard model in order to improve the agreement between the SSEC model and the experimental values of the S-parameters. The values of the extrinsic elements have been extracted with the help of short and open dummy structures and refined using the Dambrine's cold FET method. Finally, in order to obtain the values of the SSEC elements better fitting the experimental S-parameters for each gate bias, the QUCS circuit simulator has been used. The excellent agreement between the experimental values of S_{11} and S_{22} and those obtained with the SSEC model up to 67 GHz is shown in Fig. 4.

Fig. 5 shows a comparison between the SSEC extracted from the measurements and with a completely intrinsic physical models based on MC simulations. MC simulations

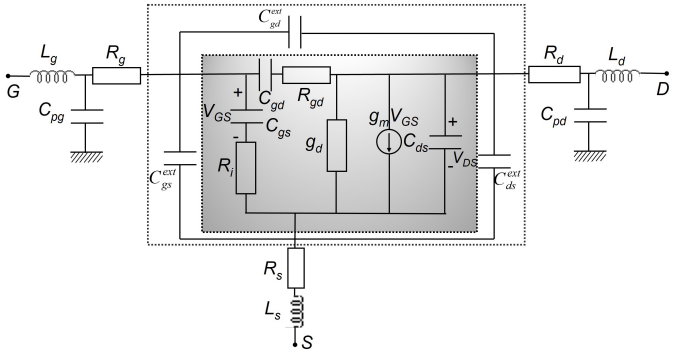

Fig. 3. Equivalent circuit of the HEMT detector, the gray box represent the intrinsic circuit. The extrinsic elements are related to the device pads.

TABLE I
VALUES OF THE EXTRINSIC ELEMENTS OF THE SSEC.

C_{pg} (fF)	8.0
C_{pd} (fF)	11.0
C_{gd}^{ext} (fF)	8.9
C_{gs}^{ext} (fF)	4.7
C_{ds}^{ext} (fF)	2.9
L_g (pH)	20.0
L_d (pH)	25.0
L_s (pH)	15.0
R_g=R_d=R_s (Ω)	1.0

precisely reproduce the I_D-V_{DS} curves of the HEMT, see Fig. 2 once the effect of source and drain contact resistances, R_s and R_d, and the Schottky barrier height at the gate metal-semiconductor junction has been analytically included in a post-processing stage. The values extracted for the SSEC capacitances as a function of V_{GS}-V_{th}, Fig. 5(a) shows a fairly good agreement, mainly for low V_{GS}. In open channel conditions the agreement is not so good due to the fact that a significant influence of R_s and R_d are not included in MC simulations, and neither the R_{gd} resistor. The good agreement between the values of the intrinsic SSEC elements from MC and from experimental S-parameters validates the accuracy of the values obtained for the extrinsic elements, shown in Table I. This will allow us to use those values for representing the extrinsic high-frequency performance of the devices taking as a base the intrinsic MC simulations by adding the effect of such parasitic elements. However, it must be done carefully, because, as shown in Fig. 6 presenting the comparison of the S-parameters provided by the experimentally-extracted SSEC model and by MC simulations up to 110 GHz, a good agreement is obtained at low frequencies but not at the highest ones. This, again, maybe due to the effect of the contact resistances, R_s and R_d, which must be included in the MC simulations.

The advantage of the SSEC model is that it is possible to obtain with a simulator such as QUCS the values of the S-parameters at frequencies above the reach from experimental measurements. Also, it allows to understand the effect of device width scaling (since the intrinsic SSEC elements are proportional to it), or the influence of external elements such as gate-drain or gate-source capacitors, typically used

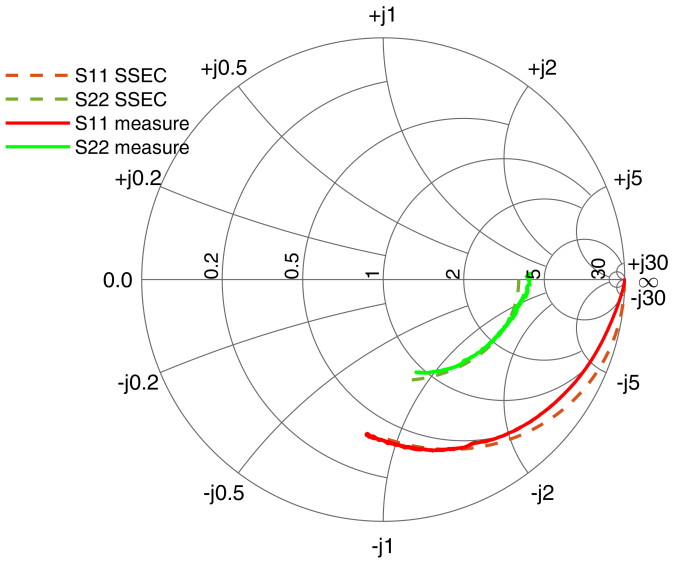

Fig. 4. Comparison of the measured (solid lines) values of S_{11} and S_{22} with those obtained with the SSEC model (dashed lines) up to 67 GHz for V_{GS}-V_{th}=0.2 V, the bias point for optimum detection. At low frequency a slight disagreement appears due to trapping effects in the GaN buffer [13].

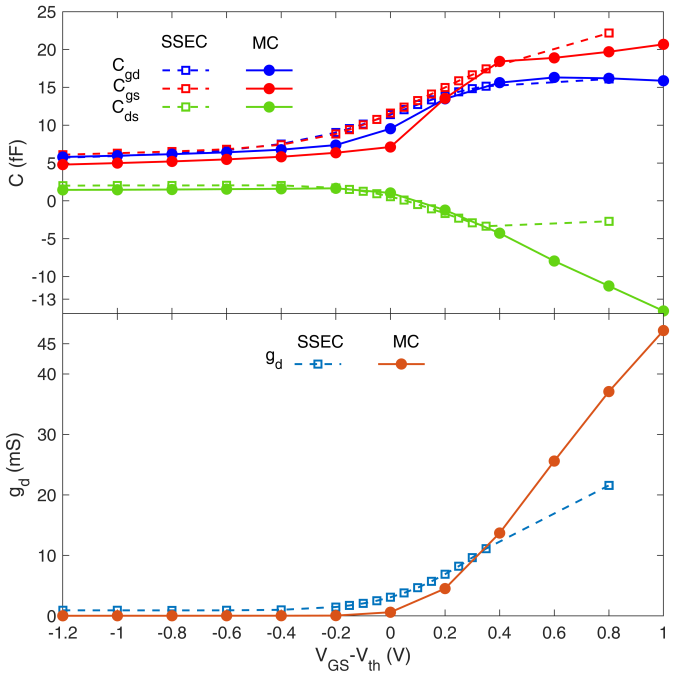

Fig. 5. (a) Comparison of the intrinsic C_{gd}, C_{gs}, C_{ds} extracted from SSEC (empty square symbols) and results of simulation MC (filled circle symbols). (b) output conductance g_d with equivalent circuit and MC simulations.

to optimize the detection performances. Some examples of its practical use will be presented at the conference.

B. Analysis of the frequency roll-off of the detection

With the recently developed closed form expression for the case of DI [7] one can obtain the responsivity β as:

$$\beta=\frac{R_0}{2}\left(g_{20}|S_{12}|^2+g_{02}|1+S_{22}|^2+2g_{11}\Re[S_{12}^*(1+S_{22})]\right) \quad (1)$$

where R_0=50 Ω is the typical output impedance of the RF power source. The coefficients g_{20}, g_{02} and g_{11} are the static conductance coefficients defined as

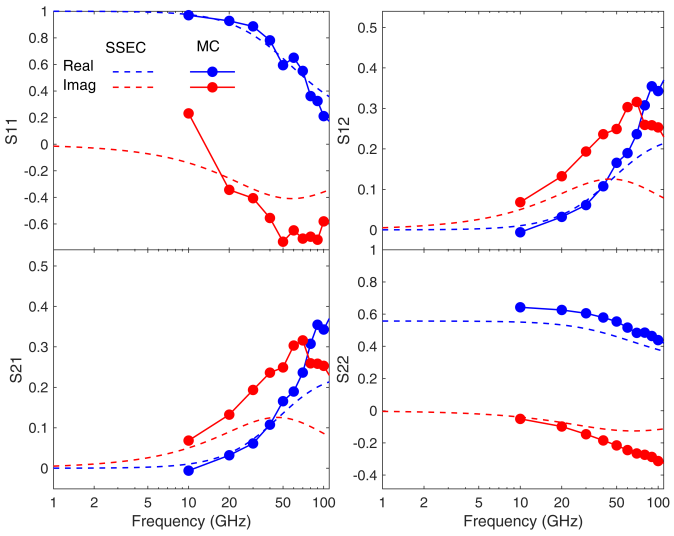

Fig. 6. Comparison of the real (blue) and imaginary (red) part of the S-parameters obtained with the SSEC model extracted from experimental measurements (dashed lines) and directly from MC simulations (solid lines with filled circle symbols) at V_{GS}-V_{th}=0.2 V.

$g_{ij}=\partial^{(i+j)}I_D/\partial^i V_{GS}\partial^j V_{DS}$ extracted from the I_D-V_{DS} curves. Fig. 7 shows the good agreement obtained between the measured values of f_{3B} and those calculated with the SSEC as a function of V_{GS}. The inset of the figure shows the absolute value of the normalized measured responsivity ($|\beta/\beta_0|$, being β_0 is the value of the responsivity at low frequency) up to 67 GHz and that calculated inserting the SSEC S-parameters in equation (1) for three selected gate biases. The value of f_{3B} is obtained applying a Lorentzian fit $1/(1+(f/f_{3dB})^2)$ to those curves. f_{3B} is around 50 GHz at the optimum detection bias point (V_{GS}=-3.6 V), and slightly decreases as the gate bias is increased. This is due to the fact that the frequency roll-off is caused by the gate-drain coupling, mainly through the C_{gd} and C_{gd}^{ext} capacitances (practically in parallel), whose added effect is pretty constant in the bias range shown in the figure (C_{gd} changes only slightly and C_{gd}^{ext} is constant).

III. Conclusions

A SSEC model for a GaN HEMT has been extracted using S-parameter measurements up to 67 GHz and compared with the results of completely intrinsic physics based MC simulations. The good agreement between both intrinsic models validates the accuracy of the determination of the parasitic elements, while the extrinsic SSEC model is able to precisely reproduce the detection performance of the device (through a closed-form expression for the responsivity, β). The frequency roll-off of $\beta(f)$ is shown to be almost independent of V_{GS} due to the fact that it is due to the gate-drain coupling, happening through the C_{gd} and C_{gd}^{ext} capacitances, whose added effect is nearly constant.

Acknowledgements

This work has been partially supported through Grant PID2020-115842RB-I00 funded by MCIN/AEI/10.13039/501100011033 and the Junta de Castilla y León and FEDER through project SA136P23. This research has made use of the high performance computing

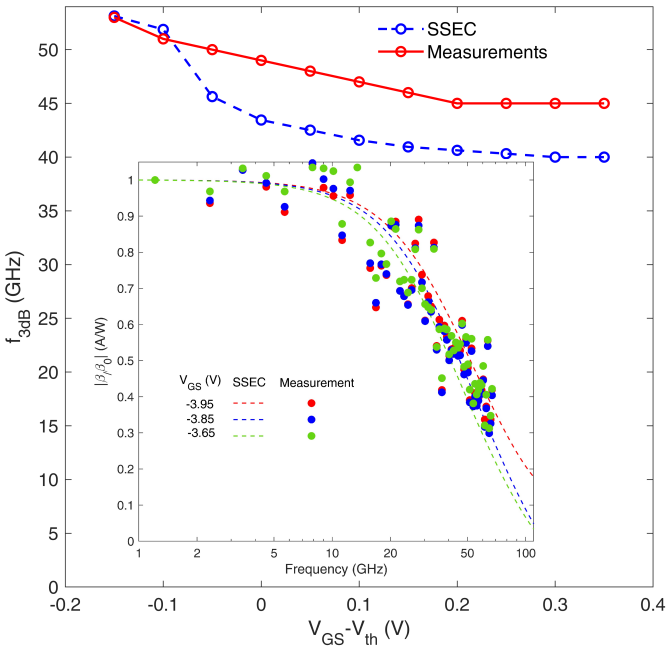

Fig. 7. Comparison of the experimental (solid line) values of f_{3dB} with those obtained with the SSEC (dashed lines) as a function of V_{GS}. The inset shows the normalized experimental responsivity (filled circles) $\beta(f)$ for selected V_{GS} values (near the bias point for maximum detection) compared with that obtained with the SSEC (dashed lines).

resources of the Castilla y León Supercomputing Center (SCAYLE, www.scayle.es), financed by the European Regional Development Fund (ERDF).

REFERENCES

[1] H. W. Hou *et al.*, "High Temperature Terahertz Detectors Realized by a GaN High Electron Mobility Transistor," *Jpn. J. Appl. Phys.,* vol. 7, no. 1, pp. 1-6, Ap. 2017.

[2] G. Paz-Martínez *et al.*, "Temperature and gate-length dependence of subthreshold RF detection in GaN HEMTs," *Sensors,* vol.22, no. 4, pp. 1515, Feb. 2022.

[3] M. Bauer *et al.*, "A high-sensitivity AlGaN/GaN HEMT terahertz detector with integrated broadband bow-tie antenna," *IEEE Trans. Terahertz Sci. Technol.,* vol. 9, no. 4, pp. 1515, Jul. 2019.

[4] M. Bauer *et al.*, "A 0.65 THz focal-plane array in a quarter-micron CMOS process technology," *IEEE Journal of Solid-State Circuits,* vol. 44, no. 7, pp. 1968–1976, Jul. 2009.

[5] F. Ludwig *et al.*, "Terahertz Detection with Graphene FETs: Photothermoelectric and Resistive Self-Mixing Contributions to the Detector Response, " *ACS Appl. Electron. Mater.*, online DOI: 10.1021/acsaelm.3c01511, 2024.

[6] G. Dambrine *et al.*, "A new method for determining the FET small-signal equivalent circuit," *IEEE Trans. Microw. Theory Techn.,* vol. 36, no. 7, pp. 1151–1159, Jul. 1988.

[7] G. Paz-Martínez *et al.*, "A Closed-Form Expression for the Frequency Dependent Microwave Responsivity of Transistors Based on the I-V Curve and S-Parameters," *IEEE Trans. Microw. Theory Techn.,* vol. 2, no. 1, pp. 415-420, Jan. 2024.

[8] J. Mateos *et al.*, "Plasma Enhanced Terahertz Rectification and Noise in InGaAs HEMTs," *IEEE Transactions on Terahertz Science and Technology,* vol. 2, no. 5, pp. 562–569, 2012.

[9] Y. Cordier *et al.*, "AlGaN/GaN HEMTs on resistive Si(111) substrate grown by gas-source MBE," *Electronics Letters,* vol. 38, pp. 91–92, Feb. 2002.

[10] S. Rennesson *et al.*, "Optimization of Al0.29Ga0.71N/GaN High Electron Mobility Heterostructures for High-Power/Frequency Performances," *IEEE Transactions on Electron Devices,* vol. 60, pp. 3105–3111, Jul. 2013.

[11] P. Altuntas *et al.*, "Power Performance at 40 GHz of AlGaN/GaN High-Electron Mobility Transistors Grown by Molecular Beam Epitaxy on Si(111) Substrate," *EEE Electron Device Letters,* vol. 36, pp. 303–305, Apr. 2015.

[12] J. Mateos *et al.*, "Design optimization of AlInAs-GaInAs HEMTs for high-frequency applications," *IEEE Transactions on Electron Devices.,* vol. 51, no. 4, pp. 521–528, Apr. 2004.

[13] S. D. Nsele *et al.*, "Broadband frequency dispersion small-signal modeling of the output conductance and transconductance in AlInN/GaN HEMTs," *IEEE Transactions on Electron Devices,* vol. 60, pp. 1372–1378, Apr. 2013.